

Article

High-temperature Spin Crossover of a Solvent-Free Iron(II) Complex with the Linear Hexadentate Ligand [Fe(L₂₋₃₋₂^{Ph})](AsF₆)₂ (L₂₋₃₋₂^{Ph} = bis[N-(1-Phenyl-1H-1,2,3-triazol-4-yl)methylidene-2-aminoethyl]-1,3-propanediamine)

Hiroaki Hagiwara 

Department of Chemistry, Faculty of Education, Gifu University, Yanagido 1-1, Gifu 501-1193, Japan; hagiwara@gifu-u.ac.jp; Tel.: +81-58-293-2253

Received: 29 December 2018; Accepted: 20 January 2019; Published: 1 February 2019



Abstract: A novel mononuclear iron(II) complex with a linear hexadentate N₆ ligand, containing two 1,2,3-triazole moieties, [Fe(L₂₋₃₋₂^{Ph})](AsF₆)₂ (**1**), was synthesized (L₂₋₃₋₂^{Ph} = bis[N-(1-Phenyl-1H-1,2,3-triazol-4-yl)methylidene-2-aminoethyl]-1,3-propanediamine). Variable-temperature magnetic susceptibility measurements revealed a gradual one-step spin crossover (SCO) between the high-spin (HS, *S* = 2) and low-spin (LS, *S* = 0) states above room temperature (*T*_{1/2} = 468 K). The spin transition was further confirmed by differential scanning calorimetry (DSC). A single-crystal X-ray diffraction study showed that the complex was in the LS state (*S* = 0) at room temperature (296 K). In the crystal lattice, a three-dimensional (3D) supramolecular network was formed by intermolecular CH⋯π and π–π interactions of neighboring complex cations [Fe(L₂₋₃₋₂^{Ph})]²⁺. AsF₆[−] ions were located interstitially in the 3D network of complex cations, with no solvent-accessible voids. The crystal structure at 448 K (mixture of HS and LS species) was also successfully determined thanks to the thermal stability of the solvent-free crystal.

Keywords: spin crossover; iron(II); mononuclear; 1,2,3-triazole; linear hexadentate ligand; spin transition; magnetism; calorimetry; crystal structure

1. Introduction

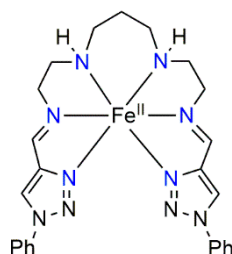
Spin-crossover (SCO) compounds are one of the most attractive candidates for molecule-based memory, switching, and sensing devices for the next generation. Their electronic configurations, i.e., high-spin (HS) and low-spin (LS) states, can be interconverted by temperature, pressure, applied magnetic field, or light irradiation [1–4]. In the past few decades, various SCO materials with different coordination architecture such as mononuclear complexes with multidentate ligands, polynuclear systems, and coordination polymers [1–3,5–19], have been developed. The SCO properties of such compounds have been investigated using various techniques, including single-crystal and powder X-ray diffraction methods, magnetic susceptibility measurements, differential scanning calorimetry (DSC), electronic, vibrational, and Mössbauer spectroscopies, and computational studies [1–3,20–28]. From a practical application point of view, an abrupt SCO at around room temperature (RT) with a wide thermal hysteresis is required [29]. The investigation of high-temperature SCO above RT is also important to produce thermally stable SCO materials under extreme conditions. While the spin transition temperature (*T*_{1/2}) is essentially related to the ligand field strength, cooperativity between SCO metal sites, through intermolecular interactions and/or bridging ligands, has a key role in controlling *T*_{1/2} as well as abruptness of spin transition and width of hysteresis. However,

to date, complexes showing SCO above 400 K remain scarce [30–35]. Tong has recently pointed out that “the main obstacles toward developing high-temperature SCO materials lie in the improper ligand-field strength and poor structural stability caused by the lattice solvents or weak supramolecular interactions” [31]. Developing solvent-free crystals is of particular importance with respect to the availability of the single-crystal X-ray diffraction method in high-temperature regions.

Recently, our group has studied N_6 -coordinated SCO iron(II) compounds bearing 1-*R*-1*H*-1,2,3-triazole-containing multidentate Schiff-base ligands such as tridentate [33], tetradentate [35,36], and tripodal hexadentate ligands [37]. Interestingly, most of these compounds showed SCO behaviors either around RT or at remarkably high temperatures. Thus, this ligand system may generally provide a strong ligand-field strength in inducing RT or high-temperature SCO. We must examine this hypothesis in other 1,2,3-triazole-containing multidentate Schiff-base ligand systems such as bidentate, pentadentate, and linear hexadentate ligands.

Linear hexadentate-ligand SCO systems are known in Iron(II) [38–44], iron(III) [45–52], and manganese(III) [53–56] complexes. They have attracted much attention since they have interesting symmetry-breaking SCO properties [39–41,43,44,49,50,56]. Iron(III) [46,51] and manganese(III) [54] complexes that show SCO-spanning around RT have been reported. There are only a few reports of linear hexadentate SCO iron(II) complexes bearing the imidazole-containing N_6 ligands H_2L^{3-2-3} [38–41,43,44] and H_2L^{2-3-2} [42] (H_2L^{3-2-3} = bis[[(2-methylimidazol-4-yl)methylidene]3-aminopropyl] ethylenediamine, H_2L^{2-3-2} = bis[*N*-(2-methylimidazol-4-yl)methylidene-2-aminoethyl]propanediamine), and all reports show SCO below RT. Of these, the highest $T_{1/2}$ is 208 K, reported for the complex $[Fe(H_2L^{2-3-2})](ClO_4)_2$ with the 2-3-2-tetramine backbone [42].

In this work, the 1,2,3-triazole moiety was introduced into a hexadentate N_6 ligand system with a 2-3-2 tetramine backbone, instead of the imidazole group of $[Fe(H_2L^{2-3-2})](ClO_4)_2$ [42], to increase $T_{1/2}$ above RT. The solvent-free complex $[Fe(L_{2-3-2}^{Ph})](AsF_6)_2$ (**1**), showing SCO above RT ($T_{1/2}$ = 468 K), was successfully synthesized (L_{2-3-2}^{Ph} = bis[*N*-(1-Phenyl-1*H*-1,2,3-triazol-4-yl)methylidene-2-aminoethyl]-1,3-propanediamine, Scheme 1). The magnetic susceptibility, DSC, and X-ray analysis of the crystal structures at 296 K (the LS state) and 448 K (mixture of HS and LS species) of **1** are reported.



Scheme 1. Schematic drawing of linear hexadentate N_6 ligand iron(II) complex-cation $[Fe(L_{2-3-2}^{Ph})]^{2+}$.

2. Results and Discussion

2.1. Synthesis and Characterization of $[Fe(L_{2-3-2}^{Ph})](AsF_6)_2$ (**1**)

The linear hexadentate N_6 ligand L_{2-3-2}^{Ph} was prepared by the 2:1 condensation reaction of 1-phenyl-1*H*-1,2,3-triazole-4-carbaldehyde and *N,N'*-bis(2-aminoethyl)-1,3-propanediamine in methanol (MeOH). The iron(II) complex **1** was prepared by mixing methanolic solutions of the ligand with $FeCl_2 \cdot 4H_2O$ and a MeOH/ H_2O mixed solution of $KAsF_6$ with a 1:1:2 molar ratio under an inert nitrogen atmosphere at ambient temperature. Dark orange-red block crystals were precipitated in one day. They were stable in the air and showed no efflorescence. The chemical formula of $[Fe(L_{2-3-2}^{Ph})](AsF_6)_2$ was confirmed by elemental analysis, thermogravimetry [TG; Figure 1a], and crystal structure analysis. These results indicated that no solvent molecules were involved in the crystal. As shown in Figure 1b, during the TG measurement, the initial dark orange-red color of the grinding samples at ambient temperature was unchanged until ~400 K, where it gradually

changed to yellow-brown between 400 and 515 K, suggesting the occurrence of SCO above RT. This yellow-brown color of the sample was retained until ~550 K, where it then turned black with an abrupt weight loss, corresponding to degradation. The phase purity of **1** was confirmed by the powder X-ray diffraction (PXRD) pattern compared to the simulated powder diffractogram from the single-crystal X-ray structural data (Figure 2). The infrared spectrum of **1** showed characteristic bands at ~1596 and 702 cm^{-1} , corresponding to the C=N stretching vibration of the Schiff-base ligand and the AsF_6^- ion, respectively [57,58].

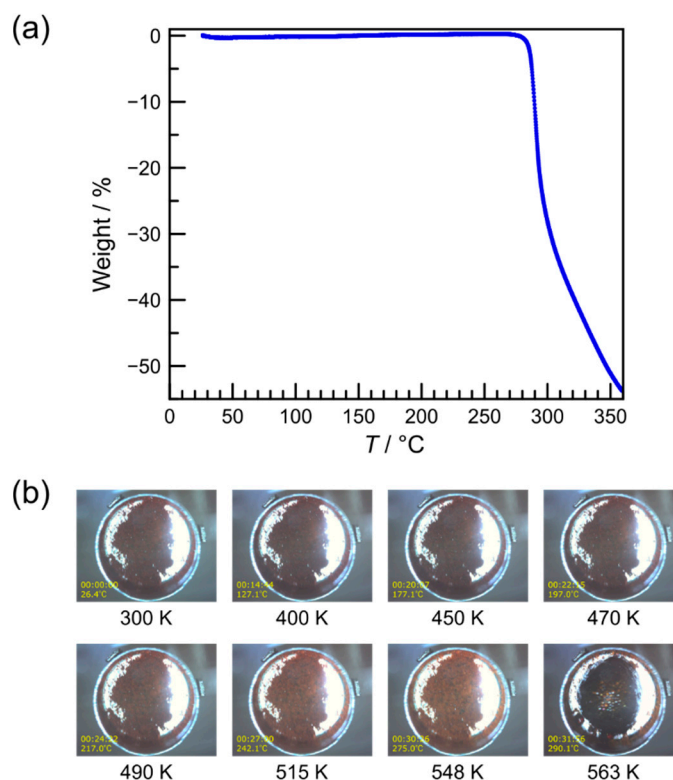


Figure 1. (a) Thermogravimetry (TG) curve of $[\text{Fe}(\text{L}_{2-3-2}^{\text{Ph}})](\text{AsF}_6)_2$ (**1**) and (b) selected real-time sample images during the TG measurement.

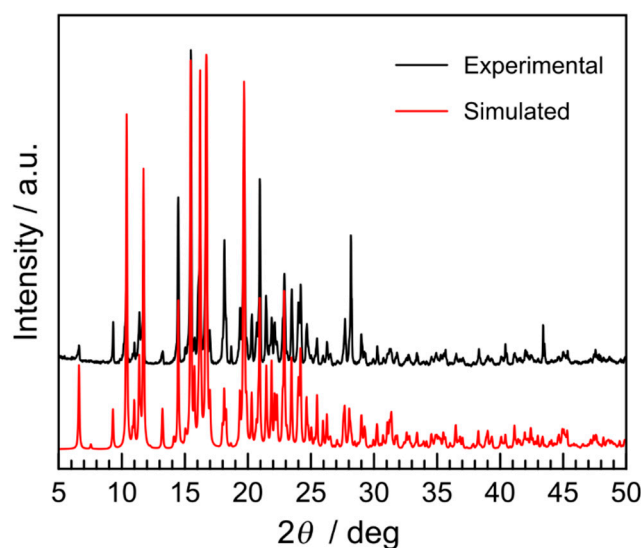


Figure 2. Experimental powder X-ray diffraction (PXRD) pattern of **1** (black) at room temperature (RT) compared with the simulated pattern from the single crystal X-ray data at 296 K (red).

2.2. Magnetic Properties of Complex 1

The magnetic susceptibilities were measured upon heating from 300 to 515 K and subsequent cooling to 300 K at a sweep rate of 1 K min^{-1} under an applied magnetic field of 1 T using a SQUID magnetometer with a special heating setup. The $\chi_M T$ versus T plots for the ground sample are shown in Figure 3, demonstrating a complete one-step SCO between HS ($S = 2$) and LS ($S = 0$) states above RT, where χ_M is the molar magnetic susceptibility, and T is the absolute temperature. The $\chi_M T$ value was $0.0 \text{ cm}^3 \text{ K mol}^{-1}$ at 300 K, which was consistent with the theoretical value for a LS Fe^{II} ($S = 0$) complex, and this $\chi_M T$ value was almost constant in the temperature region $< 380 \text{ K}$. After further raising the temperature above 380 K, the $\chi_M T$ value increased gradually to reach $\sim 3.0 \text{ cm}^3 \text{ K mol}^{-1}$ at 515 K, which was compatible with the expected value for a HS Fe^{II} ($S = 2$) complex. The magnetic behaviors were very similar in the heating and cooling modes, indicating the absence of thermal hysteresis. The SCO transition temperature ($T_{1/2}$) was found to be about 468 K. Although the gradual SCO profile of the present complex **1** was similar to that of the related complex $[\text{Fe}(\text{H}_2\text{L}^{2-3-2})](\text{ClO}_4)_2$ [42], the SCO transition temperature of **1** was considerably higher than that of $[\text{Fe}(\text{H}_2\text{L}^{2-3-2})](\text{ClO}_4)_2$ ($T_{1/2} = 208 \text{ K}$) by about 260 K, indicating that the 1,2,3-triazole-containing ligand $\text{L}_{2-3-2}^{\text{Ph}}$ gave the ligand field strength, which was stronger than that of the imidazole-containing ligand $\text{H}_2\text{L}^{2-3-2}$.

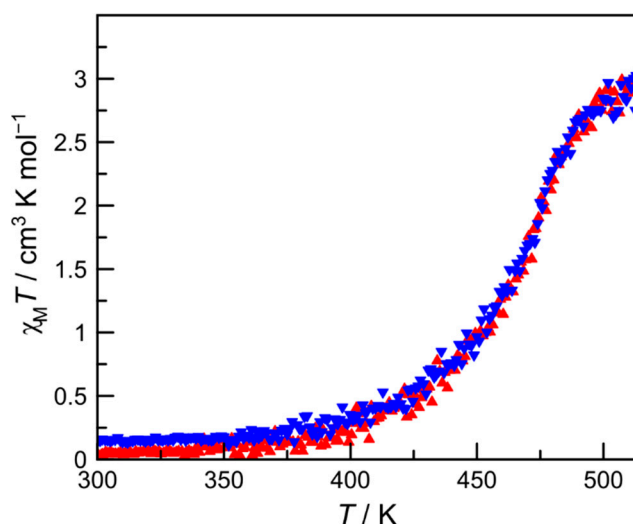


Figure 3. The magnetic behavior of **1** in the form of $\chi_M T$ vs. T plots. Complex **1** was warmed from 300 to 515 K (filled triangles; red) and then cooled from 515 to 300 K (filled inverted triangles; blue) at a sweep rate of 1 K min^{-1} .

2.3. Differential Scanning Calorimetry (DSC) of Complex 1

The DSC measurement was also carried out in the 273–518 K temperature range at a sweep rate of 5 K min^{-1} to investigate the SCO property of **1** in more detail (Figure 4). The DSC curves upon heating and cooling showed endothermic and exothermic peaks at 483 and 481 K, respectively, which were slightly higher than the $T_{1/2}$ value from the magnetic data. The corresponding enthalpy (ΔH) and entropy (ΔS) variations were $\Delta H = -21.5/19.1 \text{ kJ mol}^{-1}$ and $\Delta S = -44.4/39.7 \text{ J K}^{-1} \text{ mol}^{-1}$, respectively, which were comparable with those of typical iron(II) SCO complexes [1,3].

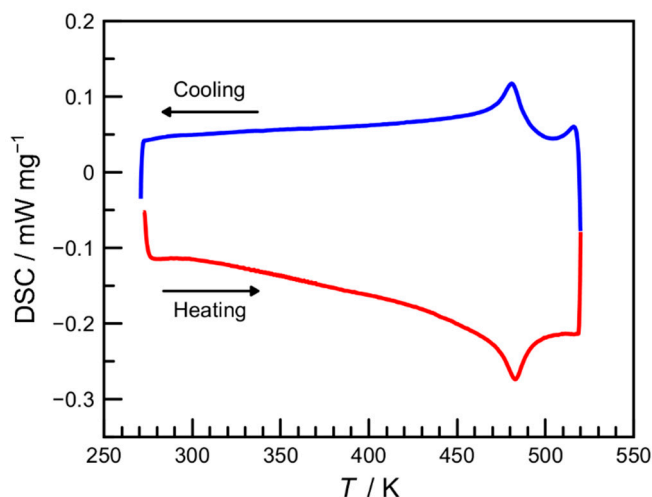


Figure 4. Differential scanning calorimetry (DSC) curves of **1** recorded over the temperature range of 273–518 K in the heating (red) and cooling (blue) modes at a sweep rate of 5 K min^{−1}.

2.4. Crystal Structure of Complex **1**

The single-crystal X-ray diffraction data for **1** were collected at 296 K (the LS state) and at 448 K (mixture of HS and LS species), where 448 K was the highest temperature limit for our diffractometer. Table 1 shows the crystallographic data, indicating that the cell dimensions at the two temperatures were similar, and no crystallographic phase transition was observed. The cell volume changed from 3506.82(18) Å³ at 448 K to 3384.98(14) Å³ at 296 K, corresponding to a volume reduction of 3.4%. This reduction was associated with a partial spin transition, from the mixture of HS and LS states (448 K) to complete LS state (296 K), as observed from the magnetic susceptibility results. Table 2 summarizes the relevant coordination bond lengths and angles, as well as additional structural parameters such as Σ [59], Θ [60], the continuous shape measures (CShMs) S(Oh) [61], and octahedral volume. The unique crystallographic unit consisted of one complex cation [Fe(L₂₋₃₋₂^{Ph})]²⁺ and two AsF₆[−] ions.

Figure 5 shows the structure of the complex cation [Fe(L₂₋₃₋₂^{Ph})]²⁺ at 296 K. The Fe^{II} ion was coordinated by N₆-donor atoms of the helically arranged linear hexadentate Schiff-base ligand L₂₋₃₋₂^{Ph} to give an octahedral coordination environment with Δ or Λ configuration. Although the complex cation depicted in Figure 5 had the Δ configuration, the complex crystallized in a centrosymmetric space group, $P2_1/n$, and complex-cations with both isomers coexisted in the crystal to form a racemic crystal. At 296 K, the Fe–N distances were in the range of 1.930(2)–2.062(3) Å. The average Fe–N distance was 1.988 Å, typical for LS Fe^{II} bound to N₆ donors. The Fe–N bond distances at 448 K (1.964(4)–2.086(3) Å) were longer than those expected for a LS Fe^{II} complex and shorter than those expected for a HS Fe^{II} complex with a similar N₆-donor ligand. It is noteworthy that the coordination bond distance of Fe–N_{imine} was shorter than that of Fe–N_{triazole} and Fe–N_{amine}. The average Fe–N bond length increased from 1.988 Å at 296 K to 2.027 Å at 448 K. The difference of 0.039 Å was considerably smaller than that found between the HS and LS states reported (ca. 0.2 Å) for the SCO Fe^{II} complexes with similar N₆-donor ligands, indicating the occurrence of a partial spin transition between 296 and 448 K. On the basis of the 0.2 Å typical difference in the average Fe–N bond length between HS and LS Fe^{II} states, about 20% of the iron centers were in the HS state at 448 K. This is roughly comparable to the HS fraction of ~31% at 448 K estimated from the magnetic results (where $\chi_M T = 3.0$ cm³ K mol^{−1} at 515 K and $\chi_M T = 0.0$ cm³ K mol^{−1} at 300 K were used as the HS and LS limiting values, respectively, and $\chi_M T = 0.94$ cm³ K mol^{−1} at 448 K). The octahedral distortion parameters Σ and Θ , the CShMs of the Fe^{II} centers relative to the ideal octahedron S(Oh), and the octahedral volume increase from 296 K to 448 K all indicated a rearrangement of the N₆ coordination environment to a more distorted octahedral geometry upon LS → HS SCO. These results were consistent with the magnetic susceptibility and DSC results. Finally, it should be noted that the Fe–N_{triazole} distances

of LS **1** at 296 K were shorter than the related Fe–N_{imidazole} distances of LS [Fe(H₂L²⁻³⁻²)](ClO₄)₂ at 150 K (2.020(2) Å) [42] by about 0.04 Å. Other Fe–N distances were almost similar to those of LS [Fe(H₂L²⁻³⁻²)](ClO₄)₂ at 150 K (Fe–N_{imine} = 1.919(2) Å and Fe–N_{amine} = 2.052(2) Å), possibly reflecting the stronger ligand field strength of **1** compared to that of [Fe(H₂L²⁻³⁻²)](ClO₄)₂.

Figure 6 shows the network structure of **1** at 296 K. As shown in Figure 6, adjacent complex cations [Fe(L₂₋₃₋₂^{Ph})]²⁺ of **1** were connected by three types of intermolecular CH···π interactions between C9–H7_{imine} and C5_{Ph}ⁱ, C14–H17_{methylene} and Cg1_{Ph}ⁱⁱ, and C19–H25_{triazole} and Cg2_{Ph}ⁱⁱⁱ, with the distances of C9–H7···C5ⁱ = 3.59 Å (C9–H7···C5ⁱ = 2.81 Å), C14–H17···Cg1ⁱⁱ = 3.55 Å (C14–H17···Cg1ⁱⁱ = 2.77 Å), and C19–H25···Cg2ⁱⁱⁱ = 3.50 Å (C19–H25···Cg2ⁱⁱⁱ = 3.07 Å), respectively (Cg1 = centroid of the C1–C6 ring, Cg2 = centroid of the C20–C25 ring, symmetry operations: i, –1 + x, y, z; ii, 3/2 – x, –1/2 + y, 1/2 – z; iii, 1 – x, 1 – y, –z). In addition, there was one intermolecular π–π interaction with the distance of Cg2···Cg2^{iv} = 3.78 Å (symmetry operation: iv, –x, 1 – y, –z), forming the three-dimensional (3D) supramolecular network in the lattice. At 448 K, this 3D structure was retained, while distances of intermolecular CH···π and π–π interactions were longer than those at 296 K (C9–H7···C5ⁱ = 3.64 Å (C9–H7···C5ⁱ = 2.87 Å), C14–H17···Cg1ⁱⁱ = 3.69 Å (C14–H17···Cg1ⁱⁱ = 2.90 Å), C19–H25···Cg2ⁱⁱⁱ = 3.56 Å (C19–H25···Cg2ⁱⁱⁱ = 3.15 Å), and Cg2···Cg2^{iv} = 3.82 Å). Finally, AsF₆[–] ions were located interstitially in the 3D supramolecular network of complex cations with several weak NH_{amine}···F and CH···F contacts. As a result, there were no solvent-accessible voids in the crystal lattice at 296 K (namely, as-synthesized crystal at RT) analyzed by the PLATON program [62]. The overall gradual SCO behavior, with no hysteresis of **1**, presumably reflected weak cooperativity between SCO metal sites in the lattice, while the SCO-active cations constructed the 3D supramolecular network through intermolecular CH···π and π–π interactions. This may be due to the packing effect with counter anions, which tightly occupy the space of the 3D network. On the basis of the potential energy wells of the HS and LS states in a configurational coordinate diagram, with the metal–ligand distance as the configuration coordinate, the condition for observing a thermal spin transition was that the zero-point energy difference between the two spin states, $\Delta E^{\circ}_{HL} = E^{\circ}_{HS} - E^{\circ}_{LS}$, was on the order of the thermally accessible energy, $k_B T$ [1,3]. Taking into consideration the previously mentioned weak cooperativity of **1**, the introduction of the 1,2,3-triazole moiety into the linear hexadentate ligand, instead of the imidazole group, substantially affected the stabilization of the LS state, corresponding to a shift of the LS potential wells to lower energies. As a result, ΔE°_{HL} increased, and the transition temperature shifted to a higher temperature region in **1**.

Table 1. X-ray crystallographic data for **1**.

Temperature/K	296	448
Formula		C ₂₅ H ₃₀ N ₁₀ As ₂ F ₁₂ Fe
Formula weight		904.28
Crystal system		monoclinic
Space group		P2 ₁ /n (No.14)
a/Å	8.8724(2)	8.9968(2)
b/Å	16.2976(4)	16.5743(6)
c/Å	23.4941(6)	23.6197(7)
β/deg	94.865(2)	95.333(2)
V/Å ³	3384.98(14)	3506.82(18)
Z	4	4
d _{calcd.} /g cm ^{–3}	1.774	1.713
μ (Mo Kα)/mm ^{–1}	2.487	2.401
R ₁ ^a (I > 2σ(I))	0.0471	0.0648
wR ₂ ^b (I > 2σ(I))	0.1300	0.1931
R ₁ ^a (all data)	0.0570	0.0879
wR ₂ ^b (all data)	0.1374	0.2163
S	1.036	1.044
CCDC number	1,887,351	1,887,352

^aR₁ = Σ||Fo| – |Fc||/Σ|Fo|. ^bwR₂ = [Σw(|Fo|² – |Fc|²)²/Σw|Fo|²]^{1/2}.

Table 2. Relevant coordination bond lengths (Å), angles (°), and structural parameters for **1**. Σ [59] and Θ [60] are angular indices characteristic for the spin state of the complex. S(Oh) is the continuous shape measures (CShMs) of the Fe^{II} centers relative to the ideal octahedron [61].

Temperature	296	448
Fe–N3	1.980(2)	2.034(3)
Fe–N4	1.930(3)	1.964(4)
Fe–N5	2.062(3)	2.078(4)
Fe–N6	2.041(2)	2.086(3)
Fe–N7	1.930(2)	1.973(3)
Fe–N8	1.986(2)	2.024(4)
Average Fe–N	1.988	2.027
N3–Fe1–N4	80.12(11)	78.67(15)
N3–Fe1–N5	161.93(11)	160.11(17)
N3–Fe1–N6	86.96(10)	87.76(14)
N3–Fe1–N7	98.13(10)	98.47(14)
N3–Fe1–N8	92.78(10)	93.32(14)
N4–Fe1–N5	81.88(12)	81.45(19)
N4–Fe1–N6	97.13(11)	98.80(16)
N4–Fe1–N7	178.24(11)	177.14(16)
N4–Fe1–N8	99.98(11)	100.86(15)
N5–Fe1–N6	96.76(10)	95.93(15)
N5–Fe1–N7	99.87(11)	101.41(18)
N5–Fe1–N8	88.88(10)	89.78(15)
N6–Fe1–N7	82.91(10)	81.14(15)
N6–Fe1–N8	162.58(10)	160.14(14)
N7–Fe1–N8	79.88(10)	79.08(15)
Σ	84.0	90.9
Θ	250.7	282.5
S(Oh)	1.748	2.131
Octahedral volume (Å ³)	10.200	10.734

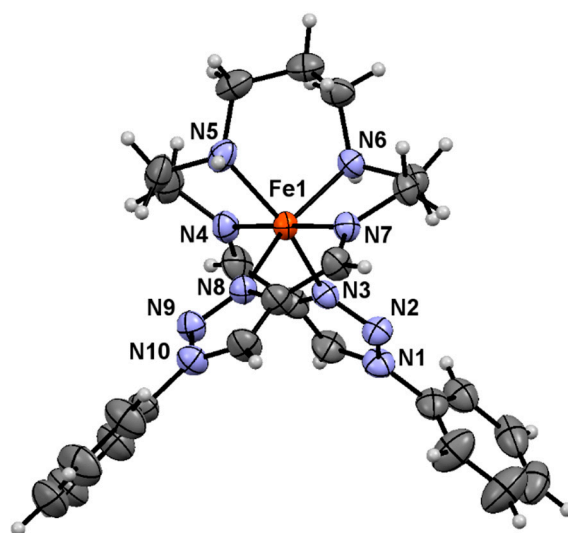


Figure 5. ORTEP drawing of the complex cation $[\text{Fe}(\text{L}_{2-3-2}^{\text{Ph}})]^{2+}$ of **1** at 296 K with the atom numbering scheme, except for carbon and hydrogen atoms, where the thermal ellipsoids are drawn with a 50% probability level.

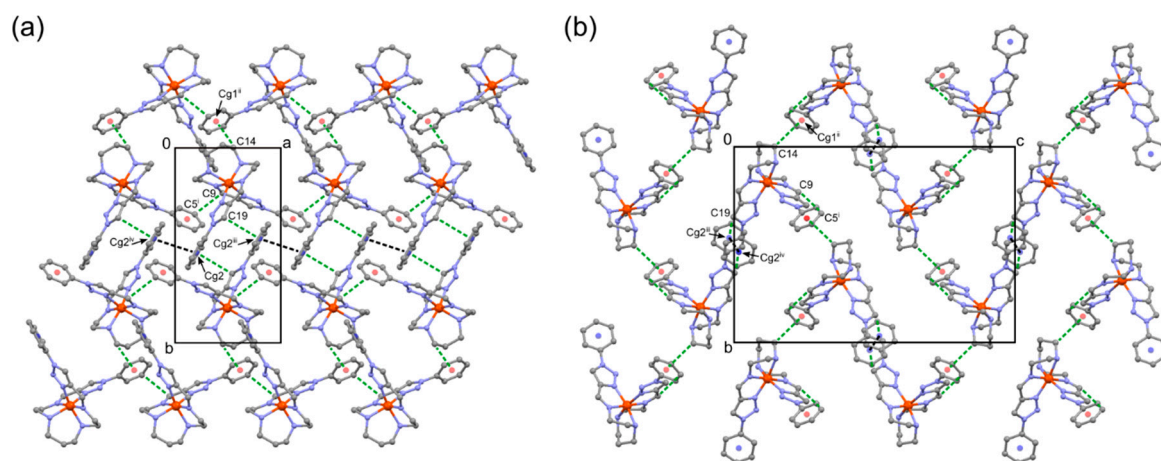


Figure 6. Molecular arrangement of **1** at 296 K, projected on the (a) *ab*-plane and (b) *bc*-plane. Adjacent complex cations $[\text{Fe}(\text{L}_{2-3-2}^{\text{Ph}})]^{2+}$ are connected by intermolecular $\text{CH} \cdots \pi$ (green dotted line) and π - π (black dotted line) interactions, forming the 3D network. Cg1 = centroid of the C1–C6 ring (transparent red) and Cg2 = centroid of the C20–C25 ring (transparent blue). Symmetry operations: (i) $-x, y, 3/2 - z$, (ii) $x, -1 + y, z$, (iii) $-x, -1 + y, 3/2 - z$, (iv) $-x, 1 - y, -z$. H atoms and AsF_6^- ions have been omitted for clarity.

3. Materials and Methods

3.1. Synthesis of the Fe^{II} Complex

3.1.1. General

All reagents and solvents were purchased from commercial sources and used for the syntheses without further purification. The compound 1-phenyl-1*H*-1,2,3-triazole-4-carbaldehyde was prepared according to methods in the literature [36,63–65]. Complexation and crystallization of **1** were performed under nitrogen atmosphere using standard Schlenk techniques. Other synthetic procedures were carried out in air.

3.1.2. Synthesis of the Linear Hexadentate N_6 Ligand $\text{L}_{2-3-2}^{\text{Ph}}$ = bis[*N*-(1-Phenyl-1*H*-1,2,3-triazol-4-yl)methylidene-2-aminoethyl]-1,3-propanediamine)

The ligand $\text{L}_{2-3-2}^{\text{Ph}}$ was prepared by mixing *N,N'*-bis(2-aminoethyl)-1,3-propanediamine and 1-phenyl-1*H*-1,2,3-triazole-4-carbaldehyde at 1:2 molar ratio in MeOH. The ligand solution thus prepared was used for the synthesis of the Fe^{II} complex without further purification and isolation.

3.1.3. Preparation of $[\text{Fe}(\text{L}_{2-3-2}^{\text{Ph}})](\text{AsF}_6)_2$ (**1**)

N,N'-bis(2-aminoethyl)-1,3-propanediamine (0.160 g, 1 mmol) in MeOH (2 mL) was added to a solution of 1-phenyl-1*H*-1,2,3-triazole-4-carbaldehyde (0.346 g, 2 mmol) in MeOH (8 mL). The resulting solution was stirred at 45 °C for 1 h. KAsF_6 (0.456 g, 2 mmol) in 6 mL of a mixed solution of MeOH, and H_2O (2/1 by volume) was added to a solution of $\text{Fe}^{\text{II}}\text{Cl}_2 \cdot 4\text{H}_2\text{O}$ (0.199 g, 1 mmol) in MeOH (4 mL); the resulting mixture was stirred at RT for 40 min. Both reaction mixtures were filtered and mixed under nitrogen atmosphere. The resulting mixture was allowed to stand for one day at RT, during which the precipitated dark orange-red block crystals were collected by suction filtration. Yield: 0.647 g (71%). Anal. Calcd for $[\text{Fe}(\text{L}_{2-3-2}^{\text{Ph}})](\text{AsF}_6)_2$ (**1**) = $\text{C}_{25}\text{H}_{30}\text{N}_{10}\text{As}_2\text{F}_{12}\text{Fe}$: C, 33.21; H, 3.34; N, 15.49. Found: C, 32.94; H, 3.24; N, 15.44%. IR (KBr): $\nu_{\text{C}=\text{N}}$ 1596, $\nu_{\text{As}-\text{F}}$ 702 cm^{-1} .

3.2. Physical Measurements

Elemental C, H, and N analyses were performed on a J-Science Lab (Kyoto, Japan) MICRO CORDER JM-10. IR spectra were recorded at RT using a JASCO (Tokyo, Japan) FT/IR 460Plus spectrophotometer with the samples prepared as KBr disks. Thermogravimetric data were collected on a Rigaku (Tokyo, Japan) Thermo plus EVO2 TG-DTA8122 instrument in the temperature range of 26–350 °C (299–623 K) at a rate of 10 K min⁻¹ under a nitrogen atmosphere (200 mL min⁻¹). Real-time sample images during thermogravimetric analysis were recorded under an optional direct monitoring system of the TG-DTA instrument. DSC measurements were performed with a Rigaku (Tokyo, Japan) Thermo plus EVO2 DSC8231 instrument over the temperature range of 273–518 K, at a sweep rate of 5 K min⁻¹ under a nitrogen atmosphere (50 mL min⁻¹), using aluminum hermetic pans with an empty pan as reference. Magnetic susceptibilities were measured in the temperature range of 300–515 K at a sweep rate of 1 K min⁻¹ under an applied magnetic field of 1 T using a Quantum Design (San Diego, CA, USA) MPMS-7 magnetometer with a special heating setup of a sample space oven option. The sample (4.70 mg) was wrapped in a homemade aluminum foil capsule (14.84 mg), mounted inside a quartz glass tube with a small amount of glass wool filler, and then fixed to the bottom of the standard sample transport rod through a copper wire. Corrections for diamagnetism of the sample were made using Pascal's constants [66,67], and a background correction for the sample holder was applied. Small disturbances were noted in the susceptibility data of higher temperature regions, which were likely from a small amount of samples being measured at high temperatures, and the effects of additional disturbances from using an aluminum foil blank. The PXRD pattern was recorded at RT on polycrystalline powders deposited on a glass plate, using a Mac Science MXP3V diffractometer at Cu K α ($\lambda = 1.5418 \text{ \AA}$) radiation operated at 1.8 kW power (40 kV, 45 mA).

3.3. Crystallographic Data Collection and Structure Analyses

X-ray diffraction data were collected by a Rigaku (Tokyo, Japan) AFC7R Mercury CCD diffractometer using graphite monochromated Mo K α radiation ($\lambda = 0.71075 \text{ \AA}$) operated at 5 kW power (50 kV, 100 mA). A single crystal was mounted on a glass fiber, and the diffraction data were collected at 296 K. Following the measurement at 296 K, the crystal was then warmed to 448 K, and the subsequent measurements were performed. The temperature of the crystal was maintained at the selected value by means of a Rigaku cooling device, with a nitrogen flow within an accuracy of ± 2 K. Data reductions and empirical absorption correction using spherical harmonics, implemented in SCALE3 ABSPACK scaling algorithm (multi-scan method) [68], were performed using the CrysAlis^{Pro} software package (version 1.171.39.46) [69]. The structures were solved by the direct method using SIR97 [70] and refined on F^2 data using the full-matrix least-squares algorithm, using SHELXL-2014 [71] with anisotropic displacement parameters for non-hydrogen atoms. Hydrogen atoms were fixed in calculated positions and refined by using a riding model. All calculations were performed by using the Yadokari-XG software package [72]. The CShMs of the Fe^{II} centers, relative to the ideal octahedron, was calculated by SHAPE 2.1 [61]. The octahedral volumes of the Fe^{II} centers were calculated by OLEX2 [73]. CCDC 1,887,351–1,887,352 contains the supplementary crystallographic data for this paper. These data can be obtained free of charge via <http://www.ccdc.cam.ac.uk/conts/retrieving.html> or from the CCDC (12 Union Road, Cambridge CB2 1EZ, UK; Fax: +44-1223-336033; E-mail: deposit@ccdc.cam.ac.uk).

4. Conclusions

In conclusion, the present iron(II) complex with the linear hexadentate N₆ ligand, containing two 1,2,3-triazole moieties [Fe(L₂₋₃₋₂^{Ph})](AsF₆)₂ (**1**), showed a high-temperature SCO with $T_{1/2} = 468$ K. The LS character and the 3D supramolecular network of the complex cations, via intermolecular CH $\cdots\pi$ and π - π interactions at RT, were confirmed by single-crystal X-ray diffraction studies at 296 K. The mixture of HS and LS species at 448 K was also structurally characterized thanks to the thermal stability of the solvent-free crystal. Surprisingly, the SCO transition temperature of

the 1,2,3-triazole-containing complex **1** was considerably higher (by about 260 K) than that of the related imidazole-containing complex $[\text{Fe}(\text{H}_2\text{L}^{2-3-2})](\text{ClO}_4)_2$ ($T_{1/2} = 208$ K) [42]. This work reveals the effectiveness of introducing a 1,2,3-triazole moiety into a linear hexadentate N_6 ligand, as well as into tridentate, tetradentate, and tripodal hexadentate N_6 -ligand systems for increasing the spin transition temperature above RT. In addition to the present linear 2-3-2-tetramine backbone, a linear 3-2-3-tetramine system is interesting, since the imidazole-containing complexes $[\text{Fe}(\text{H}_2\text{L}^{3-2-3})]\text{X}_2$ show light-induced excited spin-state trapping (LIESST) with various counter anions X, such as ClO_4 , PF_6 , AsF_6 , and SbF_6 [40,41,43,44]. Based on the present compound **1**, synthesis of analogues with other substituents, counter anions, and linear 3,2,3-tetramine backbones are now in progress. Computational and photo-magnetic studies of them are also under way. These studies will contribute towards the discovery of high-temperature and photo-active SCO materials.

Acknowledgments: This work was supported by JSPS KAKENHI Grant Number JP18K14240. A part of this work was conducted in the Institute for Molecular Science, supported by the Nanotechnology Platform Program (Molecule and Material Synthesis) of the Ministry of Education, Culture, Sports, Science and Technology (MEXT), Japan.

Conflicts of Interest: The author declares no conflict of interest.

References

1. Gütllich, P.; Goodwin, H.A. (Eds.) *Spin Crossover in Transition Metal Compounds I–III*; Topics in Current Chemistry; Springer: Berlin, Germany, 2004; Volume 233–235.
2. Halcrow, M.A. (Ed.) *Spin-Crossover Materials—Properties and Applications*; John Wiley & Sons: Chichester, UK, 2013.
3. Gütllich, P.; Gaspar, A.B.; Garcia, Y. Spin state switching in iron coordination compounds. *Beilstein J. Org. Chem.* **2013**, *9*, 342–391. [[CrossRef](#)] [[PubMed](#)]
4. Linares, J.; Codjovi, E.; Garcia, Y. Pressure and Temperature Spin Crossover Sensors with Optical Detection. *Sensors* **2012**, *12*, 4479–4492. [[CrossRef](#)] [[PubMed](#)]
5. Halcrow, M.A. The spin-states and spin-transitions of mononuclear iron(II) complexes of nitrogen-donor ligands. *Polyhedron* **2007**, *26*, 3523–3576. [[CrossRef](#)]
6. Nihei, M.; Shiga, T.; Maeda, Y.; Oshio, H. Spin crossover iron(III) complexes. *Coord. Chem. Rev.* **2007**, *251*, 2606–2621. [[CrossRef](#)]
7. Bousseksou, A.; Molnár, G.; Real, J.A.; Tanaka, K. Spin crossover and photomagnetism in dinuclear iron(II) compounds. *Coord. Chem. Rev.* **2007**, *251*, 1822–1833. [[CrossRef](#)]
8. Murray, K.S. Advances in Polynuclear Iron (II), Iron (III) and Cobalt (II) Spin-Crossover Compounds. *Eur. J. Inorg. Chem.* **2008**, 3101–3121. [[CrossRef](#)]
9. Weber, B. Spin crossover complexes with N_4O_2 coordination sphere—The influence of covalent linkers on cooperative interactions. *Coord. Chem. Rev.* **2009**, *253*, 2432–2449. [[CrossRef](#)]
10. Halcrow, M.A. Iron(II) complexes of 2,6-di(pyrazol-1-yl)pyridines—A versatile system for spin-crossover research. *Coord. Chem. Rev.* **2009**, *253*, 2493–2514. [[CrossRef](#)]
11. Aromí, G.; Barrios, L.A.; Roubeau, O.; Gamez, P. Triazoles and tetrazoles: Prime ligands to generate remarkable coordination materials. *Coord. Chem. Rev.* **2011**, *255*, 485–546. [[CrossRef](#)]
12. Hayami, S.; Komatsu, Y.; Shimizu, T.; Kamihata, H.; Lee, Y.H. Spin-crossover in cobalt(II) compounds containing terpyridine and its derivatives. *Coord. Chem. Rev.* **2011**, *255*, 1981–1990. [[CrossRef](#)]
13. Muñoz, M.C.; Real, J.A. Thermo-, piezo-, photo- and chemo-switchable spin crossover iron(II)-metallocyanate based coordination polymers. *Coord. Chem. Rev.* **2011**, *255*, 2068–2093. [[CrossRef](#)]
14. Roubeau, O. Triazole-Based One-Dimensional Spin-Crossover Coordination Polymers. *Chem. A Eur. J.* **2012**, *18*, 15230–15244. [[CrossRef](#)] [[PubMed](#)]
15. Tao, J.; Wei, R.-J.; Huang, R.-B.; Zheng, L.-S. Polymorphism in spin-crossover systems. *Chem. Soc. Rev.* **2012**, *41*, 703–737. [[CrossRef](#)] [[PubMed](#)]
16. Craig, G.A.; Roubeau, O.; Aromí, G. Spin state switching in 2,6-bis(pyrazol-3-yl)pyridine (3-bpp) based Fe(II) complexes. *Coord. Chem. Rev.* **2014**, *269*, 13–31. [[CrossRef](#)]

17. Harding, D.J.; Harding, P.; Phonsri, W. Spin crossover in iron (III) complexes. *Coord. Chem. Rev.* **2016**, *313*, 38–61. [[CrossRef](#)]
18. Attwood, M.; Turner, S.S. Back to back 2,6-bis(pyrazol-1-yl)pyridine and 2,2':6',2''-terpyridine ligands: Untapped potential for spin crossover research and beyond. *Coord. Chem. Rev.* **2017**, *353*, 247–277. [[CrossRef](#)]
19. Scott, H.S.; Staniland, R.W.; Kruger, P.E. Spin crossover in homoleptic Fe (II) imidazolylimine complexes. *Coord. Chem. Rev.* **2018**, *362*, 24–43. [[CrossRef](#)]
20. Cannizzo, A.; Milne, C.J.; Consani, C.; Gawelda, W.; Bressler, C.; van Mourik, F.; Chergui, M. Light-induced spin crossover in Fe(II)-based complexes: The full photocycle unraveled by ultrafast optical and X-ray spectroscopies. *Coord. Chem. Rev.* **2010**, *254*, 2677–2686. [[CrossRef](#)]
21. Wolny, J.A.; Diller, R.; Schünemann, V. Vibrational spectroscopy of mono- and polynuclear spin-crossover systems. *Eur. J. Inorg. Chem.* **2012**, 2635–2648. [[CrossRef](#)]
22. Wolny, J.A.; Paulsen, H.; Trautwein, A.X.; Schünemann, V. Density functional theory calculations and vibrational spectroscopy on iron spin-crossover compounds. *Coord. Chem. Rev.* **2009**, *253*, 2423–2431. [[CrossRef](#)]
23. Kitazawa, T.; Kishida, T.; Kawasaki, T.; Takahashi, M. Spin crossover behaviour in Hofmann-like coordination polymer Fe(py)₂[Pd(CN)₄] with ⁵⁷Fe Mössbauer spectra. *Hyperfine Interact.* **2017**, *238*, 65. [[CrossRef](#)]
24. Benaissa, H.; Rotaru, A.; Garcia, Y. Spin crossover in two 1D Fe(II) polymers with 1,2,4-triazole thiourea building blocks. *Hyperfine Interact.* **2018**, *239*, 37. [[CrossRef](#)]
25. Nakashima, S.; Kaneko, M.; Yoshinami, K.; Iwai, S.; Dote, H. On/off spin-crossover phenomenon and control of the transition temperature in assembled Iron(II) complexes. *Hyperfine Interact.* **2018**, *239*, 39. [[CrossRef](#)]
26. Paulsen, H.; Schünemann, V.; Wolny, J.A. Progress in Electronic Structure Calculations on Spin-Crossover Complexes. *Eur. J. Inorg. Chem.* **2013**, *2013*, 628–641. [[CrossRef](#)]
27. Kepp, K.P. Consistent descriptions of metal–ligand bonds and spin-crossover in inorganic chemistry. *Coord. Chem. Rev.* **2013**, *257*, 196–209. [[CrossRef](#)]
28. Ashley, D.C.; Jakubikova, E. Ironing out the photochemical and spin-crossover behavior of Fe(II) coordination compounds with computational chemistry. *Coord. Chem. Rev.* **2017**, *337*, 97–111. [[CrossRef](#)]
29. Brooker, S. Spin crossover with thermal hysteresis: Practicalities and lessons learnt. *Chem. Soc. Rev.* **2015**, *44*, 2880–2892. [[CrossRef](#)]
30. Bao, X.; Guo, P.-H.; Liu, W.; Tucek, J.; Zhang, W.-X.; Leng, J.-D.; Chen, X.-M.; Gural'skiy, I.; Salmon, L.; Bousseksou, A.; Tong, M.-L. Remarkably high-temperature spin transition exhibited by new 2D metal–organic frameworks. *Chem. Sci.* **2012**, *3*, 1629. [[CrossRef](#)]
31. Liu, W.; Bao, X.; Li, J.-Y.; Qin, Y.-L.; Chen, Y.-C.; Ni, Z.-P.; Tong, M.-L. High-Temperature Spin Crossover in Two Solvent-Free Coordination Polymers with Unusual High Thermal Stability. *Inorg. Chem.* **2015**, *54*, 3006–3011. [[CrossRef](#)]
32. Zheng, S.; Reintjens, N.R.M.; Siegler, M.A.; Roubeau, O.; Bouwman, E.; Rudavskiy, A.; Havenith, R.W.A.; Bonnet, S. Stabilization of the Low-Spin State in a Mononuclear Iron(II) Complex and High-Temperature Cooperative Spin Crossover Mediated by Hydrogen Bonding. *Chem. A Eur. J.* **2016**, *22*, 331–339. [[CrossRef](#)]
33. Hagiwara, H.; Tanaka, T.; Hora, S. Synthesis, structure, and spin crossover above room temperature of a mononuclear and related dinuclear double helicate iron(II) complexes. *Dalton Trans.* **2016**, *45*, 17132–17140. [[CrossRef](#)] [[PubMed](#)]
34. Hora, S.; Hagiwara, H. High-temperature Wide Thermal Hysteresis of an Iron(II) Dinuclear Double Helicate. *Inorganics* **2017**, *5*, 49. [[CrossRef](#)]
35. Hagiwara, H.; Masuda, T.; Ohno, T.; Suzuki, M.; Udagawa, T.; Murai, K. Neutral Molecular Iron(II) Complexes Showing Tunable Bistability at Above, Below, and Just Room Temperature by a Crystal Engineering Approach: Ligand Mobility into a Three-Dimensional Flexible Supramolecular Network. *Cryst. Growth Des.* **2017**, *17*, 6006–6019. [[CrossRef](#)]
36. Hagiwara, H.; Okada, S. A polymorphism-dependent $T_{1/2}$ shift of 100 K in a hysteretic spin-crossover complex related to differences in intermolecular weak CH \cdots X hydrogen bonds (X = S vs. S and N). *Chem. Commun.* **2016**, *52*, 815–818. [[CrossRef](#)] [[PubMed](#)]
37. Hagiwara, H.; Minoura, R.; Okada, S.; Sunatsuki, Y. Synthesis, Structure, and Magnetic Property of a New Mononuclear Iron(II) Spin Crossover Complex with a Tripodal Ligand Containing Three 1,2,3-Triazole Groups. *Chem. Lett.* **2014**, *43*, 950–952. [[CrossRef](#)]

38. Bréfuel, N.; Shova, S.; Tuchagues, J.-P.; Matsumoto, N. An Abrupt Spin Crossover Fe^{II} Complex Based on Homochiral Chain. *Chem. Lett.* **2005**, *34*, 1092–1093. [[CrossRef](#)]
39. Bréfuel, N.; Imatomi, S.; Torigoe, H.; Hagiwara, H.; Shova, S.; Meunier, J.-F.; Bonhommeau, S.; Tuchagues, J.-P.; Matsumoto, N. Structural–Electronic Correlation in the First-Order Phase Transition of [FeH₂L^{2-Me}](ClO₄)₂ (H₂L^{2-Me} = Bis[(2-methylimidazol-4-yl)methylidene]-3-aminopropyl)ethylenediamine). *Inorg. Chem.* **2006**, *45*, 8126–8135. [[CrossRef](#)]
40. Bréfuel, N.; Watanabe, H.; Toupet, L.; Come, J.; Matsumoto, N.; Collet, E.; Tanaka, K.; Tuchagues, J.-P. Concerted spin crossover and symmetry breaking yield three thermally and one light-induced crystallographic phases of a molecular material. *Angew. Chem. Int. Ed.* **2009**, *48*, 9304–9307. [[CrossRef](#)]
41. Bréfuel, N.; Collet, E.; Watanabe, H.; Kojima, M.; Matsumoto, N.; Toupet, L.; Tanaka, K.; Tuchagues, J.-P. Nanoscale self-hosting of molecular spin-states in the intermediate phase of a spin-crossover material. *Chem. A Eur. J.* **2010**, *16*, 14060–14068. [[CrossRef](#)]
42. Hagiwara, H.; Kawano, A.; Fujinami, T.; Matsumoto, N.; Sunatsuki, Y.; Kojima, M.; Miyamae, H. Conformational effect of a spin crossover iron(II) complex: Bis[N-(2-methylimidazol-4-yl)methylidene-2-aminoethyl]propanediamineiron(II) perchlorate. *Inorg. Chim. Acta* **2011**, *367*, 141–150. [[CrossRef](#)]
43. Collet, E.; Watanabe, H.; Bréfuel, N.; Palatinus, L.; Roudaut, L.; Toupet, L.; Tanaka, K.; Tuchagues, J.-P.; Fertey, P.; Ravy, S.; Toudic, B.; Cailleau, H. Aperiodic Spin State Ordering of Bistable Molecules and Its Photoinduced Erasing. *Phys. Rev. Lett.* **2012**, *109*, 257206. [[CrossRef](#)] [[PubMed](#)]
44. Watanabe, H.; Bréfuel, N.; Collet, E.; Toupet, L.; Tanaka, K.; Tuchagues, J.-P. Competing symmetry breaking and spin crossover in [FeH₂L^{2-Me}](ClO₄)₂. *Eur. J. Inorg. Chem.* **2013**, *1*, 710–715. [[CrossRef](#)]
45. Sinn, E.; Sim, G.; Dose, E.V.; Tweedle, M.F.; Wilson, L.J. Iron(III) chelates with hexadentate ligands from triethylenetetramine and β-diketones or salicylaldehyde. Spin state dependent crystal and molecular structures of [Fe(acac)₂trien]PF₆ (S = 5/2), [Fe(acacCl)₂trien]PF₆ (S = 5/2), [Fe(sal)₂trien]Cl·2H₂O (S = 1/2), and [Fe(sal)₂trien]NO₃·H₂O (S = 1/2). *J. Am. Chem. Soc.* **1978**, *100*, 3375–3390. [[CrossRef](#)]
46. Maeda, Y.; Oshio, H.; Tanigawa, Y.; Oniki, T.; Takashima, Y. Physical Characteristic and Molecular Structure of Spin-Crossover Iron(III) Complexes of Monoclinic Form with Hexadentate Ligands Derived from Triethylenetetramine and Salicylaldehyde [Fe(sal₂trien)]BPh₄·acetone. *Bull. Chem. Soc. Jpn.* **1991**, *64*, 1522–1527. [[CrossRef](#)]
47. Hayami, S.; Matoba, T.; Nomiyama, S.; Kojima, T.; Osaki, S.; Maeda, Y. Structures and Magnetic Properties of Some Fe(III) Complexes with Hexadentate Ligands: In Connection with Spin-Crossover Behavior. *Bull. Chem. Soc. Jpn.* **1997**, *70*, 3001–3009. [[CrossRef](#)]
48. Martinho, P.N.; Harding, C.J.; Müller-Bunz, H.; Albrecht, M.; Morgan, G.G. Inducing Spin Crossover in Amphiphilic Iron(III) Complexes. *Eur. J. Inorg. Chem.* **2010**, *2010*, 675–679. [[CrossRef](#)]
49. Griffin, M.; Shakespeare, S.; Shepherd, H.J.; Harding, C.J.; Létard, J.-F.; Desplanches, C.; Goeta, A.E.; Howard, J.A.K.; Powell, A.K.; Mereacre, V.; et al. A Symmetry-Breaking Spin-State Transition in Iron(III). *Angew. Chem. Int. Ed.* **2011**, *50*, 896–900. [[CrossRef](#)] [[PubMed](#)]
50. Vieira, B.J.C.; Coutinho, J.T.; Santos, I.C.; Pereira, L.C.J.; Waerenborgh, J.C.; da Gama, V. [Fe(nsal₂trien)]SCN, a New Two-Step Iron(III) Spin Crossover Compound, with Symmetry Breaking Spin-State Transition and an Intermediate Ordered State. *Inorg. Chem.* **2013**, *52*, 3845–3850. [[CrossRef](#)] [[PubMed](#)]
51. Fitzpatrick, A.J.; Martinho, P.N.; Gildea, B.J.; Holbrey, J.D.; Morgan, G.G. Robust Room Temperature Hysteresis in an Fe^{III} Spin Crossover Metallomesogen. *Eur. J. Inorg. Chem.* **2016**, *2016*, 2025–2029. [[CrossRef](#)]
52. Martinho, P.N.; Kühne, I.A.; Gildea, B.; McKerr, G.; O'Hagan, B.; Keyes, T.E.; Lemma, T.; Gandolfi, C.; Albrecht, M.; Morgan, G.G. Self-Assembly Properties of Amphiphilic Iron(III) Spin Crossover Complexes in Water and at the Air–Water Interface. *Magnetochemistry* **2018**, *4*, 49. [[CrossRef](#)]
53. Morgan, G.G.; Murnaghan, K.D.; Müller-Bunz, H.; McKee, V.; Harding, C.J. A Manganese(III) Complex That Exhibits Spin Crossover Triggered by Geometric Tuning. *Angew. Chem. Int. Ed.* **2006**, *45*, 7192–7195. [[CrossRef](#)] [[PubMed](#)]
54. Pandurangan, K.; Gildea, B.; Murray, C.; Harding, C.J.; Müller-Bunz, H.; Morgan, G.G. Lattice effects on the spin-crossover profile of a mononuclear manganese(III) cation. *Chem. A Eur. J.* **2012**, *18*, 2021–2029. [[CrossRef](#)] [[PubMed](#)]
55. Martinho, P.N.; Gildea, B.; Harris, M.M.; Lemma, T.; Naik, A.D.; Müller-Bunz, H.; Keyes, T.E.; Garcia, Y.; Morgan, G.G. Cooperative Spin Transition in a Mononuclear Manganese(III) Complex. *Angew. Chem.* **2012**, *124*, 12765–12769. [[CrossRef](#)]

56. Fitzpatrick, A.J.; Trzop, E.; Müller-Bunz, H.; Dîrtu, M.M.; Garcia, Y.; Collet, E.; Morgan, G.G. Electronic vs. structural ordering in a manganese(III) spin crossover complex. *Chem. Commun.* **2015**, *51*, 17540–17543. [[CrossRef](#)] [[PubMed](#)]
57. Nakamoto, K. *Infrared and Raman Spectra of Inorganic and Coordination Compounds*, 6th ed.; John Wiley & Sons: Hoboken, NJ, USA, 2009.
58. Yamada, M.; Hagiwara, H.; Torigoe, H.; Matsumoto, N.; Kojima, M.; Dahan, F.; Tuchagues, J.-P.; Re, N.; Iijima, S. A variety of spin-crossover behaviors depending on the counter anion: Two-dimensional complexes constructed by NH \cdots Cl $^-$ hydrogen bonds, [Fe^{II}H₃L^{Me}]Cl·X (X = PF₆⁻, AsF₆⁻, SbF₆⁻, CF₃SO₃⁻; H₃L^{Me} = tris[2-[(2-methylimidazol-4-yl)methylidene]amino]ethyl]amine). *Chem. A Eur. J.* **2006**, *12*, 4536–4549. [[CrossRef](#)]
59. Guionneau, P.; Marchivie, M.; Bravic, G.; Létard, J.-F.; Chasseau, D. Structural aspects of spin crossover. Examples of the [Fe^{II}L_n(NCS)₂] complexes. *Top. Curr. Chem.* **2004**, *234*, 97–128.
60. Marchivie, M.; Guionneau, P.; Létard, J.-F.; Chasseau, D. Photo-induced spin-transition: The role of the iron(II) environment distortion. *Acta Crystallogr. Sect. B* **2005**, *61*, 25–28. [[CrossRef](#)]
61. Llunell, M.; Casanova, D.; Cirera, J.; Alemany, P.; Alvarez, S. *SHAPE2.1. Program for Calculating Continuous Shape Measures of Polyhedral Structures*; Universitat de Barcelona: Barcelona, Spain, 2013.
62. Spek, A.L. Structure validation in chemical crystallography. *Acta Crystallogr. Sect. D Biol. Crystallogr.* **2009**, *65*, 148–155. [[CrossRef](#)]
63. Siddiki, A.A.; Takale, B.S.; Telvekar, V.N. One pot synthesis of aromatic azide using sodium nitrite and hydrazine hydrate. *Tetrahedron Lett.* **2013**, *54*, 1294–1297. [[CrossRef](#)]
64. Pathigoolla, A.; Pola, R.P.; Sureshan, K.M. A versatile solvent-free azide-alkyne click reaction catalyzed by in situ generated copper nanoparticles. *Appl. Catal. A Gen.* **2013**, *453*, 151–158. [[CrossRef](#)]
65. L'abbé, G.; Bruynseels, M.; Delbeke, P.; Toppet, S. Molecular rearrangements of 4-iminomethyl-1,2,3-triazoles. Replacement of 1-aryl substituents in 1 H -1,2,3-triazole-4-carbaldehydes. *J. Heterocycl. Chem.* **1990**, *27*, 2021–2027. [[CrossRef](#)]
66. Kahn, O. *Molecular Magnetism*; VCH: Weinheim, Germany, 1993.
67. Bain, G.A.; Berry, J.F. Diamagnetic Corrections and Pascal's Constants. *J. Chem. Educ.* **2008**, *85*, 532–536. [[CrossRef](#)]
68. SCALE3 ABSPACK, version: 1.0.4; gui: 1.03; an Oxford Diffraction Program; Oxford Diffraction Ltd.: Abingdon, UK, 2005.
69. Rigaku Oxford Diffraction. *CrysAlisPro Software System*, version 1.171.39.46; Rigaku Corporation: Oxford, UK, 2018.
70. Altomare, A.; Burla, M.C.; Camalli, M.; Casciarano, G.L.; Giacovazzo, C.; Guagliardi, A.; Moliterni, A.G.G.; Polidori, G.; Spagna, R. SIR97: A new tool for crystal structure determination and refinement. *J. Appl. Crystallogr.* **1999**, *32*, 115–119. [[CrossRef](#)]
71. Sheldrick, G.M. Crystal structure refinement with SHELXL. *Acta Crystallogr. Sect. C Struct. Chem.* **2015**, *71*, 3–8. [[CrossRef](#)] [[PubMed](#)]
72. Wakita, K. Yadokari-XG, Software for Crystal Structure Analyses, 2001; Release of Software (Yadokari-XG 2009) for Crystal Structure Analyses: Kabuto, C.; Akine, S.; Nemoto, T.; Kwon, E.J. *Cryst. Soc. Jpn.* **2009**, *51*, 218–224.
73. Dolomanov, O.V.; Bourhis, L.J.; Gildea, R.J.; Howard, J.A.K.; Puschmann, H. OLEX2: A complete structure solution, refinement and analysis program. *J. Appl. Crystallogr.* **2009**, *42*, 339–341. [[CrossRef](#)]

